



Article

Electrospun Bimetallic NiCr Nanoparticles@Carbon Nanofibers as an Efficient Catalyst for Hydrogen Generation from Ammonia Borane

Robert M. Brooks¹, Ibrahim M. Maafa^{2,*}, Abdullah M. Al-Enizi^{3,*}, M. M. El-Halwany⁴, Mohd Ubaidullah³ and Ayman Yousef^{2,5,*}

¹ Department of Civil and Environmental Engineering, Temple University, 1947 N. 12th Street, Philadelphia, PA 19122, USA

² Department of Chemical Engineering, Faculty of Engineering, Jazan University, Jazan 45142, Saudi Arabia

³ Department of Chemistry, College of Science, King Saud University, Riyadh 11451, Saudi Arabia

⁴ Department of Engineering Mathematics and Physics, Faculty of Engineering, Mansoura University, El-Mansoura 35516, Egypt

⁵ Department of Mathematics and Physics Engineering, Faculty of Engineering at Mataria, Helwan University, Cairo 11718, Egypt

* Correspondence: imoafa@jazanu.edu.sa (I.M.M.); amenizi@ksu.edu.sa (A.M.A.-E.); ayman.youssef@m-eng.helwan.edu.eg (A.Y.)

Received: 24 June 2019; Accepted: 23 July 2019; Published: 28 July 2019



Abstract: In this study, we report on the fabrication and utilization of NiCr alloy nanoparticles (NPs)-decorated carbon nanofibers (CNFs) as efficient and competent non-precious catalysts for the hydrolytic dehydrogenation of ammonia borane (AB) at 25 ± 2 °C. The introduced NFs have been fabricated in one step using a high-temperature thermal decomposition of the prepared electrospun nanofiber mats (nickel acetate tetrahydrate, chromium acetate dimer, and polyvinyl alcohol) in an inert atmosphere. The chemical composition of the NFs with different proportions of $\text{Ni}_{1-x}\text{Cr}_x$ ($x = 0.0, 0.1, 0.15, 0.2, 0.25, 0.3$) was established via standard characterization techniques. These techniques proved the formation of disorder Cr_2Ni_3 alloy and carbon for all the formulations. The as-synthesized composite NFs exhibited a higher catalytic performance for AB dehydrogenation than that of Cr-free Ni–CNFs. Among all the formulations, the sample composed of 15% Cr shows the best catalytic performance, as more H_2 was released in less time. Furthermore, it shows good stability, as it is recyclable with little decline in the catalytic activity after six cycles. It also demonstrates the activation energy, entropy (ΔS), and enthalpy (ΔH) with 37.6 kJ/mole, 0.094 kJ/mole, and 35.03 kJ/mole, respectively. Accordingly, the introduced catalyst has a lower price with higher performance encouraging a practical sustainable H_2 energy application from the chemical hydrogen storage materials.

Keywords: nanofibers; hydrogen production; energy application; electrospinning

1. Introduction

The fast growth of the global population associated with social development and technologies requires a sufficient and sustainable energy supply. For this purpose, H_2 has been adopted as one of the perfect substitute energy carriers. During storage, transit and utilization H_2 causes safety problems. Thus, the storage of hydrogen in solid form overcomes these issues. Boron-hydrides (e.g., NaBH_4 , NH_3BH_3 , LiBH_4 , etc.) are the best candidates for solid hydrogen storage as per the United States Department of Energy (US DOE) [1]. They have the potential for strengthening the hydrogen economy over time [2,3]. Their distinct features (e.g., high storage capacity (10–20 wt%) nonflammable, and

nontoxic) make them a splendid alternative for the petroleum industry as fuel [4]. Ammonia boron (AB, NH_3BH_3) has high hydrogen storage capacity (19.6 wt%) with a low molecular weight (30.86 g mol^{-1}) relative to other boron-hydrides. In the presence of a suitable catalyst, H_2 can be produced from AB at room temperature to directly power the fuel cells for a cheaper and more convenient generation of electricity and hot water without additional efforts. A suitable, low cost, and efficient catalyst is considered the major obstacle for improving the kinetic properties under moderate conditions, and consequently the wide practical application of this system. A wide range of catalysts with different structures has been used in the hydrolysis process of AB. Noble metals (e.g., Pt, Ru, and Rh) are being used for the rapid production of hydrogen on account of having excellent durability, stability, performance, and tolerance against deactivation [5–7].

However, the higher cost and resource shortages limited their practical applications. Subsequently, the search for the recyclable and low-cost catalyst has become imperative for solving these issues. The cost-efficient first-row transition metals (e.g., cobalt (Co), nickel (Ni), Copper (Cu), and iron (Fe)) are available in abundance [8–15]. Among them, Ni NPs served as the most attractive and active catalysts in the catalytic hydrolysis of AB [9,16–21]. This is because of their environmental benignity, good performance, and room temperature ferromagnetic properties [22–25]. Moreover, Ni NPs tend to easily oxidize in air or aqueous solution; they also easily aggregate and fuse, owing to their magnetic-induced property and increased surface energy [9,19,22]. These issues not merely limit their catalytic activity level; they also sharply reduce the recycling performance. Several strategies have been investigated to stabilize Ni NPs and achieve higher H_2 generation rates. These strategies include the supported Ni on the various matrices (e.g., foams, thin film, metal oxides, metal organic frameworks, etc.) [16,19,21,26–33]. Compared with the above supporters, nanocarbon materials provide a desirable surface to obtain a good attachment [34–37]. Furthermore, they have a good chemical stability, thermal stability, and adsorption capacity. Among the carbon nanostructures, CNFs have a higher surface area and more facile preparation compared to other nanocarbon materials. Many techniques have been used to produce nanofibers. Amongst these techniques, the simple electrospinning technique is considered the most suitable one due to its large production capacity at a low price [2,20]. The formed electrospun NFs containing a nanoporous structure facilitate the reactants entering and product leaving. Accordingly, CNFs easily adsorb the AB for contacting the catalyst surface and the facile releasing of H_2 . Our previous works exhibit that CNFs can assist with dispersing and stabilizing the transition metal NPs, and can be used for various applications (e.g., fuel cells and hydrogen production) [25,38].

Another strategy is the addition of an atomic diffusion barrier (e.g., Cr, Mo, and W) to Ni atoms [39]. It is considered an active route for enhancing the catalytic properties via inhibiting the agglomeration phenomena [39]. Li et al. reported that the addition of a small concentration of Cr or W to Co–B reveals a high hydrogenation activity for glucose [40]. Patel et al. [41] demonstrated that the addition of atomic diffusion barrier (e.g., Cr, Mo, and W) had a strong impact on the catalytic activity and performance of Co–B for sodium borohydride hydrolysis. In addition, Chen et al. [42] indicated that the Mo and W enhanced the activity and selectivity of Ni–B toward p-chloronitrobenzene hydrogenation. Recently, Kangkang Yang et al. [39] found that the addition of Cr, Mo, and W enhanced the catalytic activity of Ni NPs toward ammonia borane and hydrazine borane dehydrogenation.

Herein, we prepared bimetallic NiCr alloy NPs decorated within the surface of CNFs via an electrospinning technique for the first time. The prepared NFs showed excellent stability and good catalytic activity toward hydrogen generation from AB. Furthermore, NFs reveal a good stability.

2. Experimental Section

2.1. Chemicals Used

Polyvinyl alcohol (PVA) (MW = 65,000 g/mol) was obtained from the D C Chemical Company, Seoul, South Korea. Chromium acetate dimer (CrAc), nickel acetate tetrahydrate (NiAc), and ammonia

borane complex (AB) were from Sigma Aldrich, St. Louis, MO, USA. Deionized water (DI) was utilized as a solvent.

2.2. Preparation of Catalytic Nano-Fibers

Typically, 10 wt% of PVA solution was prepared by dissolving PVA granules in DI water at 50 °C with vigorously stirring. Stock solution (NiAc/PVA) was made by mixing the prepared NiAc and PVA aqueous solutions (weigh ratio 1:3). An amount from CrAc aqueous solution was added to 20 mL of NiAc/PVA aqueous solution to obtain different solutions at the mixture-composed weight ratios of CrAc to NiAc 10 wt%, 15 wt%, 20 wt%, and 30 wt%, respectively. The final solutions were stirred at 60 °C for 6 h, and then cooled at room temperature for obtaining a clear sol–gel. The sol–gel was electrospun by using 22 kV of DC power supply with a tip-to-collector distance of 20 cm. Fabricated NFs were collected from a rotating cylinder wrapped with a polyethylene sheet. The obtained electrospun NF mats were dried overnight under a vacuum at 50 °C. Finally, the mats were sintered under an Ar atmosphere for 5 h at 800 °C with the heating rate of 3 °C/min.

2.3. Catalytic Hydrolysis of Ammonia Borane Complex

The catalytic performance of the prepared NFs in the AB dehydrogenation was conducted on a gas volumetric apparatus (water-filled gas burette system). The setup of the apparatus can be found elsewhere [4,14,15,20,43]. Typically, a reactor was set up containing 10 mL of aqueous solution and 100 mM (31.5 mg) of AB. The solution in the reactor was stirred by a Teflon-coated stirring bar in the presence of a determined amount of catalytic NFs. The evolved H₂ was measured by the water replacement method. The rate of H₂ evolved was studied at different catalyst concentrations to find the rate of the reaction. Furthermore, the activation energy involved in the catalytic hydrolysis was calculated by the catalytic performance at different temperatures. In order to change the temperature, the reactor was put on a bath that contained silicon oil with a temperature regulator. Also, the stability of NFs in the AB dehydrogenation at room temperature was studied. A controlled experiment was also conducted on the similar reaction conditions without any catalytic material. It was noted that no considerable hydrogen gas evolved in the controlled experiment.

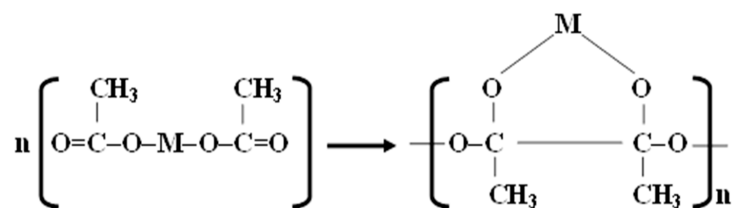
2.4. Characterization Performed

The prepared catalysts were characterized using standard techniques such as A JEOL JSM-5900 scanning electron microscope (JEOL Ltd., Tokyo, Japan) and field-emission scanning electron microscope (FESEM, Hitachi S-7400, Tokyo, Japan), which were used to study the surface morphology of the fabricated catalysts. Powder X-ray diffraction (PXRD) (Rigaku Co., Tokyo, Japan) with Cu K α ($\lambda = 1.54056 \text{ \AA}$) radiation was utilized to examine the phase and crystallinity of the prepared catalysts. A JEOL JEM-2200FS transmission electron microscope (TEM) operated at 200 kV and equipped with EDX (JEOL Ltd., Tokyo, Japan) was used to obtain high-resolution images [2,7].

3. Results

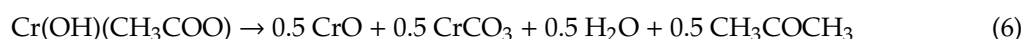
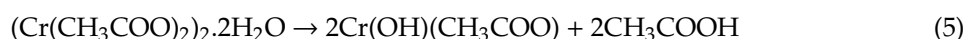
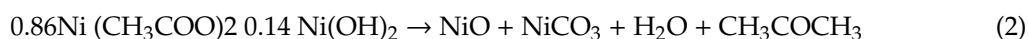
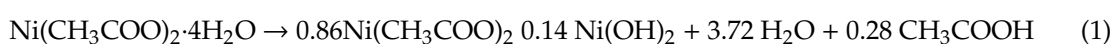
3.1. Physicochemical Characterization

Electrospinning is a powerful technique in the fabrication of inorganic NFs either from solutions or melts. The inorganic NFs fabrication process used a solution that consists of metal acetates or metal alkoxides as precursors. Polymers have been shown to have more simple polycondensation characteristics with metal acetates than those of alkoxides [2]. Furthermore, the electrospun solution that consisted of metal acetate showed an excellent morphology in the final product. The polycondensation process can be explained, as shown in Scheme 1.



Scheme 1. Polycondensation of the metal acetate precursors (M can be Ni or Cr).

The decomposition process of the precursor salts consist of metal acetates at high temperature under vacuum, and in the presence of an inert gas led to the generation of reducing gases (e.g., Co and H₂), which result from the decomposition of acetate anions. The formed gases reduced the salt and metal oxides to form pure Ni and Cr and/or their alloys rather than their oxides [2]. The formation of Ni and Cr can be defined by the following reactions [44,45]:



Various metal acetates have been applied to produce inorganic NFs with good morphology. Herein, the NiAc, CrAc, and PVA appear to have a good electrospun NF mats morphology, as shown in the SEM image (Figure 1a,b) after vacuum drying. The nanofibrous morphology of the sintered electrospun NF mats was not affected by the high calcination temperature. This may be attributed to the polycondensation of the NiAc and CrAc with PVA [3,20,44,46]. Figure 1c,d shows the sintered NFs obtained after the abnormal calcination of electrospun NF mats composed of NiAc/CrAc/PVA. It was observed in the figure that the NFs are cross-linked, and a net-like structure with some NPs is distributed on the rough surface. The formed fiber was decorated within the well-dispersed NPs.

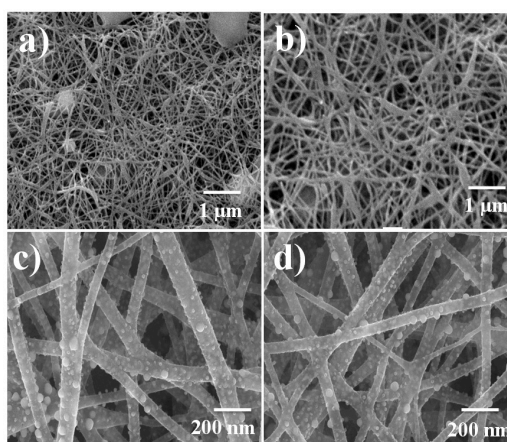


Figure 1. SEM image of electrospun NiAc/CrAc/PVA nanofiber (NF) mats after vacuum drying; (a) and (b), and field-emission scanning electron microscope (FESEM) image of the sintered powder sample; (c) and (d).

3.2. Crystal Structure

The analytical analysis of the chemical composition of the produced NFs was achieved using an XRD technique (Figure 2). Nickel and chromium are in the same row and neighbors in the periodic table. They can form a solid solution until 30 wt% at room temperature, while above this value, an eutectic solution is formed. Accordingly, the identification peaks in the XRD database are overlapped. Moreover, the formed NiCr alloys have dissimilar crystal structures compared to the pure metals. For instance, nickel can be identified in the XRD pattern if peaks are detected at 2θ values of 44.5° , 51.8° , and 76.4° corresponding to (111), (200), and (220) crystal planes, respectively (JCDPS #04-0850). However, chromium can be identified in the XRD pattern if peaks are detected at 2θ values of 44.4° , 64.6° , and 81.72° matching to (110), (200), and (211) crystal planes, respectively (JCDPS #06-0694). Interestingly, the obtained 2θ values at 43.9° , 51.2° , and 75.7° match well with (111), (200), and (220) of Cr_2Ni_3 (JCPDS # 65-629; Cr_2Ni_3) [47]. The same results were obtained for all formulations. According to the higher melting point of the two metals, 1455°C and 1907°C for Ni and Cr, respectively, than the used calcination temperature, vaporization of the produced bimetal is not predictable. Moreover, the nickel precursor represented a high amount in the initial electrospun solution compared to chromium; thus, the detected peaks in the XRD pattern (Figure 2) can be consigned to free Ni and a Cr_2Ni_3 alloy. It is worth noting that pure nickel and the bimetallic alloy can combine in the same nanoparticle, which was verified by the TEM EDX study below. Furthermore, a peak can be observed at $2\theta \sim 26^\circ$, representing an experimental d spacing of 3.37, which confirmed the presence of graphite-like carbon (d (002), PDF#; 41-1487). According to our previous studies, Ni NPs and its alloys have vital roles in the catalytic transformation of polymer NFs into graphite-like carbon during the calcination process [2,46,48,49]. These results suggested a successful formation of Cr_2Ni_3 alloy NPs@CNFs.

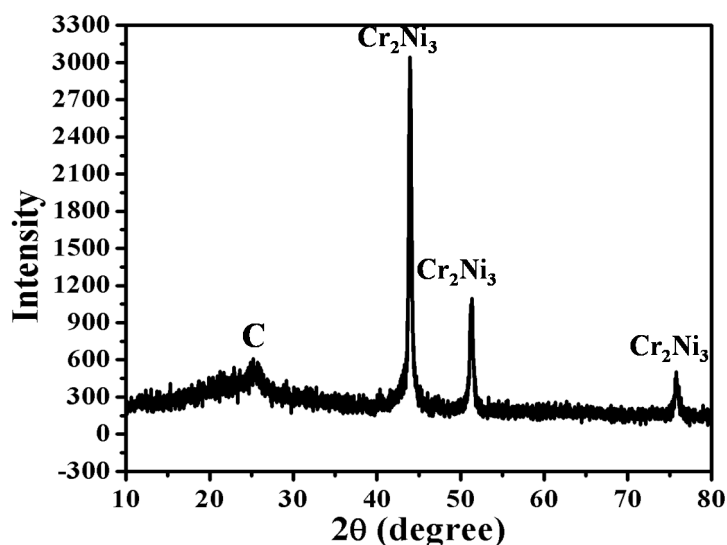


Figure 2. X-ray diffraction (XRD) pattern for the electrospun NiAc/CrAc/PVA NF mats after calcination at 800°C in inert atmosphere.

3.3. Internal Structure

A typical TEM image of nanofibers (NFs) is presented in Figure 3a. It is clear that numerous dark spots from NPs are consistently anchored and distributed on the rough surface of NFs. HRTEM images are used to determine the crystalline of the produced NFs (Figure 3b,c). The clear appearance of the distance between the parallel crystal planes in Figure 3b,c affirmed that the NPs are crystalline, while the carbon is amorphous. The distance between two parallel crystals planes is mostly the same in the NPs in Figure 3b; this confirmed the presence of one phase only, as mentioned in the XRD analysis. Accordingly, the crystalline NPs and NFs matrix can be assigned to the detected Cr_2Ni_3 NPs and graphite, respectively.

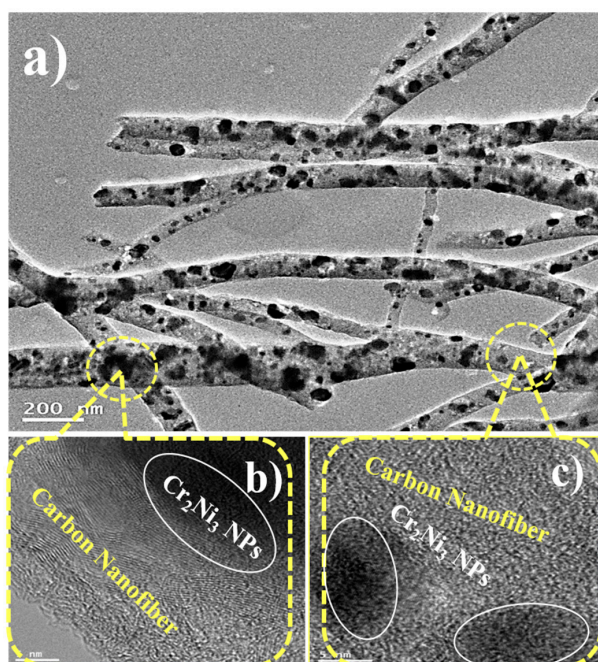


Figure 3. Normal TEM (a), and HRTEM images (b,c) of the as-synthesized Cr_2Ni_3 NPs@CNFs.

To confirm the aforementioned result, the TEM-EDX was performed to check the elements and chemical composition of the obtained NFs. The STEM results (Figure 4a) show that the NPs are encapsulated inside the NFs matrix. TEM-EDX analysis corresponding to the line shown in Figure 4a, as shown in Figure 4b–d, indicates that the Ni and Cr nanoparticles (NPs) are uniformly distributed along the chosen line in the specified area, yielding the same distribution of Ni and Cr, which indicates the alloy formation. This verifies the XRD result regarding the formation of the Cr_2Ni_3 phase. Accordingly, the formed NPs and NFs were assigned to the Cr_2Ni_3 alloy and CNFs, respectively. Moreover, Cr_2Ni_3 NPs were packed well into a thin crystalline CNF layer. The layer was present at all points along the chosen line. Carbon could enhance the catalytic activity, material conductivity, and stability. Moreover, CNFs have high adsorptive capacity, which increases the attachment of the target with the catalytic material and easily creates an outlet product due to the porosity.

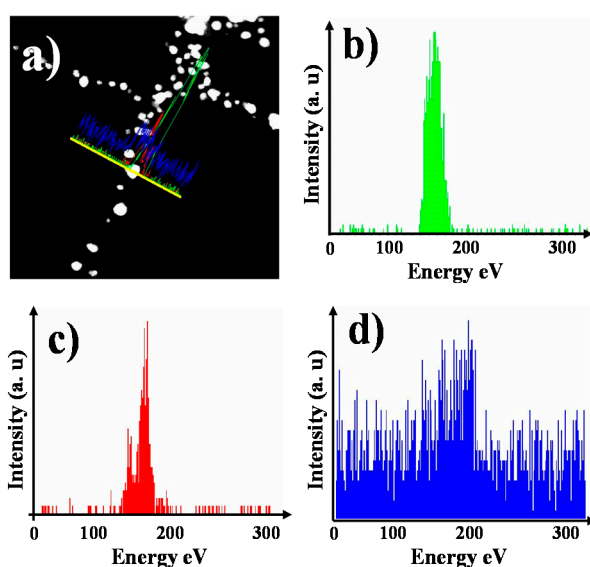


Figure 4. TEM EDX studies of Cr_2Ni_3 nanoparticles at carbon nanofibers (NPs@CNFs); STEM image, (a); Ni distribution, (b); Cr distribution, (c); and C distribution, (d).

3.4. Hydrogen Release from Ammonia Borane Complex

The synthesized $\text{Ni}_x\text{Cr}_{1-x}$ NPs–CNFs were tested as catalysts for the AB dehydrogenation. Figure 5 shows plots of the time versus equivalent H_2 (n_{H_2} mol/ n_{AB} mol) for the AB dehydrogenation in the presence of all the formulations and Ni–CNFs at the same molar ratio from the active catalyst and same concentration of AB at room temperature. As shown in the figure, the introduced NFs showed a higher catalytic performance for H_2 generation compared to the pure metallic NPs (Ni–CNFs). This may be ascribed to the synergistic effect of the introduced alloy NPs. The pure metallic NPs took a relatively longer experimental time of 27 min to release 2 mol of H_2 /1 mol of AB. The hydrogen release rate increased and the duration time decreased as the amount of Cr increased, as the most of the reaction's stoichiometric H_2 was released. The sample composed of 15 wt% Cr took a shorter time to release stoichiometric H_2 compared to the other formulations. In addition, it was observed in the figure that the H_2 generation is directly proportional to the AB dehydrogenation duration time. This good performance can be attributed to the CNFs. The CNFs have a high absorptive capacity, a high surface area, and interact with a good dispersion of active catalysts, which creates a large number of active sites. It is well known that the electrospun CNFs have the well nanoporous structure, which facilitates the contact between the reactants and the active metals as well as H_2 evolution. Accordingly, nanofibrous morphology introduced a high surface area and active sites for AB dehydrogenation. The performance can also be associated with the addition of Cr to Ni, which increases the surface area and works as an atomic barrier between Ni atoms for preventing agglomeration. Furthermore, the interaction between Ni and Cr species modified the electronic structure of the alloy [39].

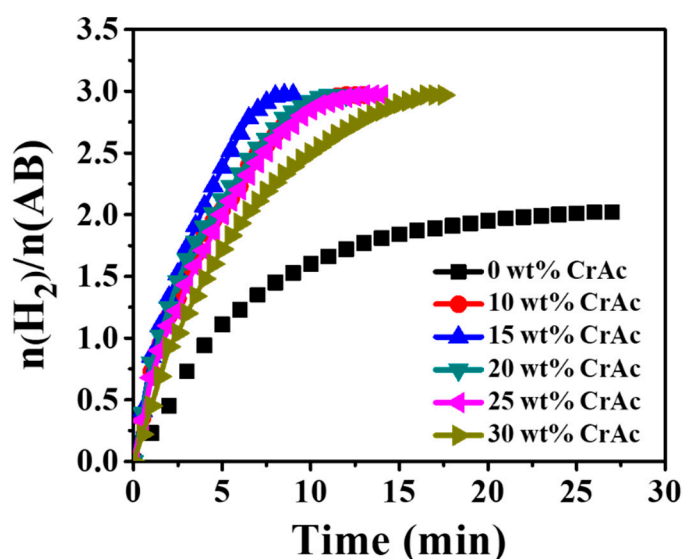


Figure 5. Evolution of H_2 gas by the hydrolytic dehydrogenation of AB in the presence of Cr_2Ni_3 NPs@CNFs with different CrAc compositions.

Accordingly, the migration electrons from Cr to Ni enhance the active sites with the electron-enriched Ni NPs. These electrons enhance the detachment of H_2 atoms from the catalyst surface. However, the increase of the Cr concentration and decrease of the H_2 release could be due to the screening of the Ni active sites, which reduces the electron transfer. Furthermore, the decrease in the H_2 generation at a Cr concentration lower than that of 15 wt% CrAc may be due to the surface oxidation.

Figure 6 demonstrates the graphs of (n_{H_2} /1 mole AB) versus the duration time of aqueous AB hydrolysis (31.5 mg and room temperature) in the presence of different concentrations of the introduced NFs (15 wt% sample). As shown in the figure, with an increase in the catalyst and the AB ratio, the time required for H_2 generation decreases. From the linear portion of the different concentrations, a graph between the log H_2 generation rates versus log catalyst concentration was plotted. From this graph,

a straight line within a slope of 0.997 was obtained, indicating that the AB hydrolysis followed a pseudo-first-order reaction with respect to the concentration of the introduced NFs (Figure 6b).

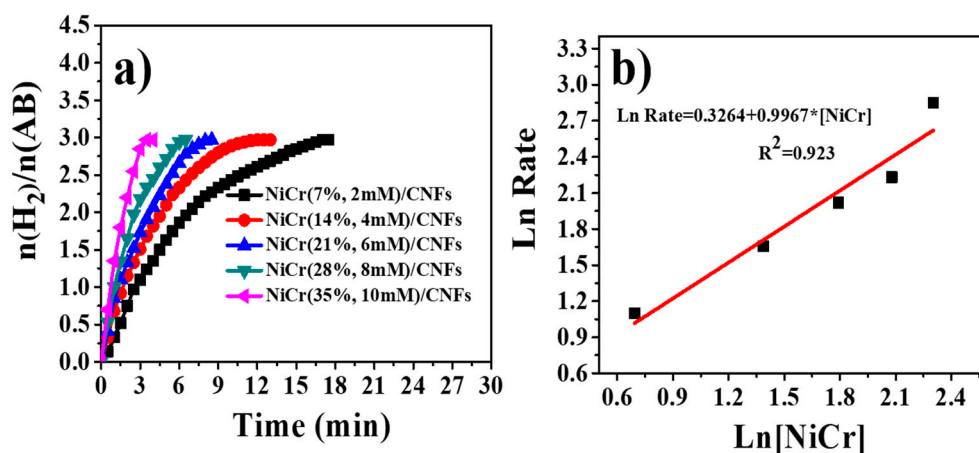


Figure 6. Effect of [Cr₂Ni₃] (15 wt% CrAc) on H₂ gas generation from hydrolytic dehydrogenation of AB (100 mM) at 25 °C (a) and Ln rate vs. Ln [Cr₂Ni₃] (b).

The effect of AB concentration (100–500 mM) on the rate of H₂ generation was also investigated. As shown in Figure 7, most of the stoichiometric hydrogen was evolved for each concentration. The logarithmic rate constant obtained from the linear portion of concentration (Figure 7b) was plotted versus logarithmic AB concentrations, and the slope was to be found to be -0.0979 , demonstrating that the hydrolysis reaction followed the zero-order reaction with respect to the AB concentration.

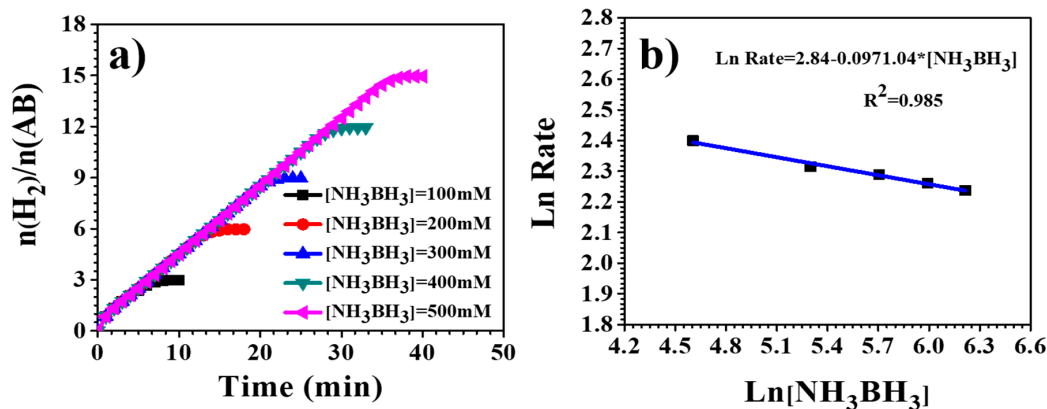


Figure 7. Effect of [NH₃BH₃] on H₂ gas generation from the hydrolytic dehydrogenation of AB using Cr₂Ni₃ NPs@ CNFs (a) and Ln Rate vs. Ln [NH₃BH₃] (b).

To determine the reaction activation energy (E_a), activation entropy (ΔS), and activation enthalpy (ΔH), the hydrolytic reaction was carried out at different temperatures ranging from 298 K to 323 K. As shown in Figure 8, as expected, the duration time for H₂ generation was reduced from 12.5 min to 3.5 min with an increasing chemical reaction temperature from 298 K to 323 K, respectively. The constant rate (k) value was determined from the linear portion from Figure 8a. The E_a , ΔS , and ΔH of the reaction were determined from the Arrhenius and Eyring plots (Figure 8a,b), and were found to be 37.6, 0.094, and 35.03 kJ/mol, respectively. Here, the obtained E_a value is comparable to the Ni-based catalyst values reported in the literature (Table 1), indicating the superior catalytic performance of the introduced NFs (15 wt%, sample). In addition, the TOF was determined to evaluate the catalytic activity, and was found to be 5.78 mol H₂ min⁻¹ (mol metal⁻¹). This value is also comparable to values

reported in the literature for Ni-based catalysts (Table 1), indicating the high activities of the introduced NFs (15 wt%, sample).

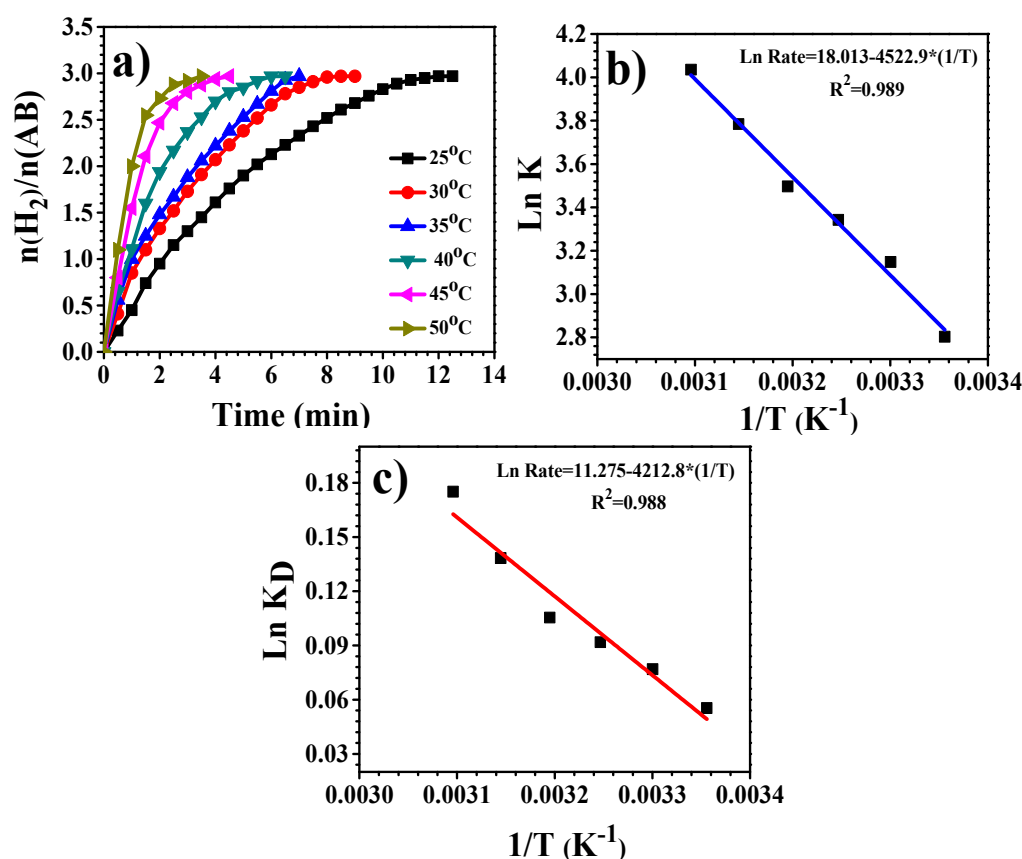


Figure 8. Evolution of H₂ gas by the hydrolytic dehydrogenation of ammonia borane (AB) in the presence of Cr₂Ni₃ NPs@CNFs (15 wt% CrAc) at different temperatures (a), the plot of ln K vs. (1/T) (b) and the plot of ln K_D vs. (1/T) (c).

Table 1. Comparison of activation energies and TOFs of different Ni-based catalysts for the hydrolytic dehydrogenation of AB.

Catalyst	E _a (KJ/mol)	TOF (mol _{H₂} · Mol _{metal} ⁻¹ · min ⁻¹)	References
Ni NPs	41.5	8.8	[17]
Ni/ZIF-8	41.5-	14.2	[28]
Fe-Ni alloy	41.5-	10.7	[12]
CoNi/graphene	13.49	16.4	[50]
Cu _{0.64} Ni _{0.36} /TiO ₂ nanotubes	36.14	15.9	[51]
Ni/BN	61.1	1.03	[52]
NiP/rGO	34.7	13.3	[22]
CuNi-MIL-101	32.2	20.9 (Cu)	[53]
Cu _{0.2} Ni _{0.8} /MCM41	38	10.7	[23]
CuNi@carbon	28.9	0.2	[20]
Cr ₂ Ni ₃ @carbon	37.6	5.78	This study

The reusability test is very significant for the practical applications of catalysts. In the present work, the reusability test of a 15 wt% CrAc sample was conducted for the hydrolytic reactions of AB. After the complete hydrolysis of AB (31.5 mg, 3n_{H₂}/1n_{AB}), the catalyst was decanted from the solution via centrifugation, washed with deionized (DI) water, and then, the reactivate catalyst was again dispersed in the same solution with the addition of the same amount of AB for the next cycle. As shown in Figure 9, the catalytic activities of the catalyst indicate stability for two runs. However, a gradual

decline was observed from the third cycle, reaching about 65% at the fifth cycle, demonstrating that the catalyst had a good reusability in the AB dehydrogenation at room temperature. The decline of catalytic activity may be attributed to the following: (1) the partial clustering of the metal NPs, (2) the increase of the solution viscosity, and (3) the passivation of the NFs' surface, which was attributed to the accumulate boron products (e.g., metaborate) on the reaction solution and catalyst surface that inhibited the metal active sites [39,49].

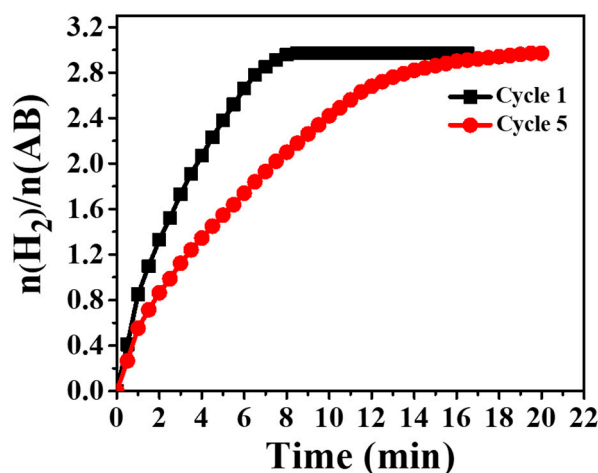


Figure 9. The catalytic performance of Cr₂Ni₃ NPs@CNFs (15 wt% CrAc at 25 °C) during recycling.

4. Conclusions

In summary, we successfully prepared metallic Cr₂Ni₃ alloy nanoparticles-decorated carbon nanofibers via the abnormal sintering of electrospun nanofiber mats composed of nickel acetate tetrahydrate, chromium acetate monohydrate, and poly(vinyl alcohol) in the argon atmosphere. The synthesized nanofibers exhibited excellent catalytic activity for the hydrolytic dehydrogenation of AB compared to the Cr-free nanofibers. The sample content 15 wt% CrAc reveals the best catalytic performance among other formulations due to its lower duration time on the H₂ generation from an aqueous solution of AB. The selected alloy shows a lower TOF and activation energy as compared to those available in the literature. The introduced catalytic NFs show a good stability in the hydrolytic dehydrogenation of AB. Accordingly, the optimum time was 3.5 min at 323 K to obtain 3 mole H₂ using 15 wt% CrAc.

Author Contributions: R.M.B. planned the experimental work, wrote the manuscript, and helped in the analysis. I.M.M. helped in the experimental work, helped in the analysis, explained the results, and writing of original draft manuscript. A.M.A.-E. helped in the analysis explained the results, and writing of original draft manuscript. M.M.E.-H. helped in explained the results and manipulated the data results. M.U. helped in the experimental work, analysis, and writing the original draft manuscript. A.Y. planned the experimental work, wrote the manuscript, helped in the analysis, explained the results, and manipulated the data results.

Acknowledgments: The authors gratefully acknowledge the Deanship of Scientific Research, King Saud University for the financial support provided through research group NO (RG-1435-010).

Conflicts of Interest: The authors declare no conflict of interest.

References

- Demirci, U.B.; Miele, P. Sodium borohydride versus ammonia borane, in hydrogen storage and direct fuel cell applications. *Energy Environ. Sci.* **2009**, *2*, 627–637. [[CrossRef](#)]
- Barakat, N.A.; El-Newehy, M.H.; Yasin, A.S.; Ghouri, Z.K.; Al-Deyab, S.S. Ni&Mn nanoparticles-decorated carbon nanofibers as effective electrocatalyst for urea oxidation. *Appl. Catal. A Gen.* **2016**, *510*, 180–188.

3. Barakat, N.A.; Motlak, M.; Elzatahry, A.A.; Khalil, K.A.; Abdelghani, E.A. Ni x Co 1–X alloy nanoparticle-doped carbon nanofibers as effective non-precious catalyst for ethanol oxidation. *Int. J. Hydrogen Energy* **2019**, *39*, 305–316. [[CrossRef](#)]
4. Patel, N.; Miotello, A. Progress in Co–B related catalyst for hydrogen production by hydrolysis of boron-hydrides: A review and the perspectives to substitute noble metals. *Int. J. Hydrogen Energy* **2015**, *40*, 1429–1464. [[CrossRef](#)]
5. Yang, X.; Cheng, F.; Liang, J.; Tao, Z.; Chen, J. PtxNi 1–X nanoparticles as catalysts for hydrogen generation from hydrolysis of ammonia borane. *Int. J. Hydrogen Energy* **2009**, *34*, 8785–8791. [[CrossRef](#)]
6. Yao, C.; Zhuang, L.; Cao, Y.; Ai, X.; Yang, H. Hydrogen release from hydrolysis of borazane on Pt-and Ni-based alloy catalysts. *Int. J. Hydrogen Energy* **2008**, *33*, 2462–2467. [[CrossRef](#)]
7. Yousef, A.; Brooks, R.M.; El-Halwany, M.; Obaid, M.; El-Newehy, M.H.; Al-Deyab, S.S.; Barakat, N.A. A novel and chemical stable Co–B nanoflakes-like structure supported over titanium dioxide nanofibers used as catalyst for hydrogen generation from ammonia borane complex. *Int. J. Hydrogen Energy* **2016**, *41*, 285–293. [[CrossRef](#)]
8. Li, J.; Zhu, Q.L.; Xu, Q. Non-noble bimetallic CuCo nanoparticles encapsulated in the pores of metal–organic frameworks: Synergetic catalysis in the hydrolysis of ammonia borane for hydrogen generation. *Catal. Sci. Technol.* **2015**, *5*, 525–530. [[CrossRef](#)]
9. Metin, Ö.; Özkar, S. Water soluble nickel(0) and cobalt(0) nanoclusters stabilized by poly(4-styrenesulfonic acid-co-maleic acid): Highly active, durable and cost effective catalysts in hydrogen generation from the hydrolysis of ammonia borane. *Int. J. Hydrogen Energy* **2011**, *36*, 1424–1432. [[CrossRef](#)]
10. Wang, H.; Zhou, L.; Han, M.; Tao, Z.; Cheng, F.; Chen, J. CuCo nanoparticles supported on hierarchically porous carbon as catalysts for hydrolysis of ammonia borane. *J. Alloys Compd.* **2015**, *651*, 382–388. [[CrossRef](#)]
11. Xu, Q.; Chandra, M. Catalytic activities of non-noble metals for hydrogen generation from aqueous ammonia–borane at room temperature. *J. Power Sources* **2006**, *163*, 364–370. [[CrossRef](#)]
12. Yan, J.-M.; Zhang, X.-B.; Han, S.; Shioyama, H.; Xu, Q. Magnetically recyclable Fe–Ni alloy catalyzed dehydrogenation of ammonia borane in aqueous solution under ambient atmosphere. *J. Power Sources* **2009**, *194*, 478–481. [[CrossRef](#)]
13. Yan, J.M.; Zhang, X.-B.; Shioyama, H.; Xu, Q. Room temperature hydrolytic dehydrogenation of ammonia borane catalyzed by Co nanoparticles. *J. Power Sources* **2010**, *195*, 1091–1094. [[CrossRef](#)]
14. Yousef, A.; Barakat, N.A.; El-Newehy, M.H.; Ahmed, M.; Kim, H.Y. Catalytic hydrolysis of ammonia borane for hydrogen generation using Cu (0) nanoparticles supported on TiO₂ nanofibers. *Colloids Surf. A Physicochem. Eng. Asp.* **2015**, *470*, 194–201. [[CrossRef](#)]
15. Yousef, A.; Barakat, N.A.; Kim, H.Y. Electrospun Cu-doped titania nanofibers for photocatalytic hydrolysis of ammonia borane. *Appl. Catal. A Gen.* **2013**, *467*, 98–106. [[CrossRef](#)]
16. Lai, Q.; Aguey-Zinsou, K.-F.; Demirci, U.B. Nanosizing ammonia borane with nickel–An all-solid and all-in-one approach for H₂ generation by hydrolysis. *Int. J. Hydrogen Energy* **2018**, *43*, 14498–14506. [[CrossRef](#)]
17. Metin, O.; Mazumder, V.; Ozkar, S.; Sun, S. Monodisperse nickel nanoparticles and their catalysis in hydrolytic dehydrogenation of ammonia borane. *J. Am. Chem. Soc.* **2010**, *132*, 1468–1469. [[CrossRef](#)]
18. Nirmala, R.; Kim, H.Y.; Yi, C.; Barakat, N.A.; Navamathavan, R.; El-Newehy, M. Electrospun nickel doped titanium dioxide nanofibers as an effective photocatalyst for the hydrolytic dehydrogenation of ammonia borane. *Int. J. Hydrogen Energy* **2012**, *37*, 10036–10045. [[CrossRef](#)]
19. Umegaki, T.; Yan, J.M.; Zhang, X.-B.; Shioyama, H.; Kuriyama, N.; Xu, Q. Preparation and catalysis of poly (N-vinyl-2-pyrrolidone)(PVP) stabilized nickel catalyst for hydrolytic dehydrogenation of ammonia borane. *Int. J. Hydrogen Energy* **2009**, *34*, 3816–3822. [[CrossRef](#)]
20. Yousef, A.; Barakat, N.A.; El-Newehy, M.; Kim, H.Y. Chemically stable electrospun NiCu nanorods@ carbon nanofibers for highly efficient dehydrogenation of ammonia borane. *Int. J. Hydrogen Energy* **2012**, *37*, 17715–17723. [[CrossRef](#)]
21. Zahmakıran, M.; Ayvalı, T.; Akbayrak, S.; Çalışkan, S.; Çelik, D.; Özkar, S. Zeolite framework stabilized nickel (0) nanoparticles: Active and long-lived catalyst for hydrogen generation from the hydrolysis of ammonia-borane and sodium borohydride. *Catal. Today* **2011**, *170*, 76–84. [[CrossRef](#)]

22. Du, X.; Yang, C.; Zeng, X.; Wu, T.; Zhou, Y.; Cai, P.; Cheng, G.; Luo, W. Amorphous NiP supported on rGO for superior hydrogen generation from hydrolysis of ammonia borane. *Int. J. Hydrogen Energy* **2017**, *42*, 14181–14187. [[CrossRef](#)]
23. Lu, Z.H.; Li, J.; Feng, G.; Yao, Q.; Zhang, F.; Zhou, R.; Tao, D.; Chen, X.; Yu, Z. Synergistic catalysis of MCM-41 immobilized Cu–Ni nanoparticles in hydrolytic dehydrogenation of ammonia borane. *Int. J. Hydrogen Energy* **2014**, *39*, 13389–13395. [[CrossRef](#)]
24. Roy, B.; Manna, J.; Sharma, P. Effect of Ni-alloys on thermal decomposition of ammonia borane. *J. Alloys Compd.* **2015**, *645*, 234–238. [[CrossRef](#)]
25. Wu, Y.; Wu, X.; Liu, Q.; Huang, C.; Qiu, X. Magnetically recyclable Ni@ h-BN composites for efficient hydrolysis of ammonia borane. *Int. J. Hydrogen Energy* **2017**, *42*, 16003–16011. [[CrossRef](#)]
26. Jiang, H.L.; Umegaki, T.; Akita, T.; Zhang, X.B.; Haruta, M.; Xu, Q. Bimetallic Au–Ni nanoparticles embedded in SiO₂ nanospheres: Synergetic catalysis in hydrolytic dehydrogenation of ammonia borane. *Chem. A Eur. J.* **2010**, *16*, 3132–3137. [[CrossRef](#)]
27. Lai, S.W.; Lin, H.-L.; Lin, Y.P.; Yu, T.L. Hydrolysis of ammonia–borane catalyzed by an iron–nickel alloy on an SBA-15 support. *Int. J. Hydrogen Energy* **2013**, *38*, 4636–4647. [[CrossRef](#)]
28. Li, P.Z.; Aranishi, K.; Xu, Q. ZIF-8 immobilized nickel nanoparticles: Highly effective catalysts for hydrogen generation from hydrolysis of ammonia borane. *Chem. Commun.* **2012**, *48*, 3173–3175. [[CrossRef](#)]
29. Li, P.Z.; Aijaz, A.; Xu, Q. Highly Dispersed Surfactant-Free Nickel Nanoparticles and Their Remarkable Catalytic Activity in the Hydrolysis of Ammonia Borane for Hydrogen Generation. *Angew. Chem. Int. Ed.* **2012**, *51*, 6753–6756. [[CrossRef](#)]
30. Metin, Ö.; Özkar, S.; Sun, S. Monodisperse nickel nanoparticles supported on SiO₂ as an effective catalyst for the hydrolysis of ammonia-borane. *Nano Res.* **2010**, *3*, 676–684. [[CrossRef](#)]
31. Ozay, O.; Inger, E.; Aktas, N.; Sahiner, N. Hydrogen production from ammonia borane via hydrogel template synthesized Cu, Ni, Co composites. *Int. J. Hydrogen Energy* **2011**, *36*, 8209–8216. [[CrossRef](#)]
32. Umegaki, T.; Yan, J.M.; Zhang, X.B.; Shioyama, H.; Kuriyama, N.; Xu, Q. Hollow Ni–SiO₂ nanosphere-catalyzed hydrolytic dehydrogenation of ammonia borane for chemical hydrogen storage. *J. Power Sources* **2009**, *191*, 209–216. [[CrossRef](#)]
33. Zhou, L.; Zhang, T.; Tao, Z.; Chen, J. Ni nanoparticles supported on carbon as efficient catalysts for the hydrolysis of ammonia borane. *Nano Res.* **2014**, *7*, 774–781. [[CrossRef](#)]
34. Cao, N.; Luo, W.; Cheng, G. One-step synthesis of graphene supported Ru nanoparticles as efficient catalysts for hydrolytic dehydrogenation of ammonia borane. *Int. J. Hydrogen Energy* **2013**, *38*, 11964–11972. [[CrossRef](#)]
35. Cao, N.; Su, J.; Luo, W.; Cheng, G. Hydrolytic dehydrogenation of ammonia borane and methylamine borane catalyzed by graphene supported Ru@ Ni core–shell nanoparticles. *Int. J. Hydrogen Energy* **2014**, *39*, 426–435. [[CrossRef](#)]
36. Yang, L.; Luo, W.; Cheng, G. Graphene-supported Ag-based core–shell nanoparticles for hydrogen generation in hydrolysis of ammonia borane and methylamine borane. *ACS Appl. Mater. Interfaces* **2013**, *5*, 8231–8240. [[CrossRef](#)]
37. Zhang, J.; Chen, C.; Yan, W.; Duan, F.; Zhang, B.; Gao, Z.; Qin, Y. Ni nanoparticles supported on CNTs with excellent activity produced by atomic layer deposition for hydrogen generation from the hydrolysis of ammonia borane. *Catal. Sci. Technol.* **2016**, *6*, 2112–2119. [[CrossRef](#)]
38. Huang, C.; Chen, C.; Ye, X.; Ye, W.; Hu, J.; Xu, C.; Qiu, X. Stable colloidal boron nitride nanosheet dispersion and its potential application in catalysis. *J. Mater. Chem. A* **2013**, *1*, 12192–12197. [[CrossRef](#)]
39. Yang, K.; Yao, Q.; Huang, W.; Chen, X.; Lu, Z.H. Enhanced catalytic activity of NiM (M= Cr, Mo, W) nanoparticles for hydrogen evolution from ammonia borane and hydrazine borane. *Int. J. Hydrogen Energy* **2017**, *42*, 6840–6850. [[CrossRef](#)]
40. Li, H.; Li, H.; Wang, M. Glucose hydrogenation over promoted Co–B amorphous alloy catalysts. *Appl. Catal. A Gen.* **2001**, *207*, 129–137. [[CrossRef](#)]
41. Patel, N.; Fernandes, R.; Miotello, A. Promoting effect of transition metal-doped Co–B alloy catalysts for hydrogen production by hydrolysis of alkaline NaBH₄ solution. *J. Catal.* **2010**, *271*, 315–324. [[CrossRef](#)]
42. Chen, L.F.; Chen, Y.W. Effect of additive (W, Mo, and Ru) on Ni–B Amorphous alloy catalyst in hydrogenation of p-chloronitrobenzene. *Ind. Eng. Chem. Res.* **2006**, *45*, 8866–8873. [[CrossRef](#)]
43. Barakat, N.A. Catalytic and photo hydrolysis of ammonia borane complex using Pd-doped Co nanofibers. *Appl. Catal. A Gen.* **2013**, *451*, 21–27. [[CrossRef](#)]

44. Mohamed, I.M.; Motlak, M.; Fouad, H.; Barakat, N.A. Cobalt/Chromium Nanoparticles-Incorporated Carbon Nanofibers as Effective Nonprecious Catalyst for Methanol Electrooxidation in Alkaline Medium. *Nano* **2016**, *11*, 1650049. [[CrossRef](#)]
45. Yousef, A.; Brooks, R.M.; El-Newehy, M.H.; Al-Deyab, S.S.; Kim, H.Y. Electrospun Co-TiC nanoparticles embedded on carbon nanofibers: Active and chemically stable counter electrode for methanol fuel cells and dye-sensitized solar cells. *Int. J. Hydrogen Energy* **2017**, *42*, 10407–10415. [[CrossRef](#)]
46. Yousef, A.; Akhtar, M.S.; Barakat, N.A.M.; Motlak, M.; Yang, O.B.; Kim, H.Y. Effective NiCu NPs-doped carbon nanofibers as counter electrodes for dye-sensitized solar cells. *Electrochim. Acta* **2013**, *102*, 142–148. [[CrossRef](#)]
47. Guanglin, N.; Yiwang, B.; Detian, W.; Xiaogen, L. Effect of Atomization Gases on the Elastic Modulus of Thermal-sprayed NiCr Coatings. *Rare Met. Mater. Eng.* **2018**, *47*, 1025–1030. [[CrossRef](#)]
48. Yousef, A.; Brooks, R.M.; Abdelkareem, M.A.; Khamaj, J.A.; El-Halwany, M.; Barakat, N.A.; L-Newehy, M.H.E.; Kim, H.Y. Electrospun NiCu Nanoalloy Decorated on Carbon Nanofibers as Chemical Stable Electrocatalyst for Methanol Oxidation. *ECS Electrochem. Lett.* **2015**, *4*, 51–55. [[CrossRef](#)]
49. Yousef, A.; Brooks, R.M.; El-Halwany, M.M.; Abutaleb, A.; El-Newehy, M.H.; Al-Deyab, S.S.; Kim, H.Y. Electrospun CoCr7C3-supported C nanofibers: Effective, durable, and chemically stable catalyst for H₂ gas generation from ammonia borane. *Mol. Catal.* **2017**, *434*, 32–38. [[CrossRef](#)]
50. Feng, W.; Yang, L.; Cao, N.; Du, C.; Dai, H.; Luo, W.; Cheng, G. In situ facile synthesis of bimetallic CoNi catalyst supported on graphene for hydrolytic dehydrogenation of amine borane. *Int. J. Hydrogen Energy* **2014**, *39*, 3371–3380. [[CrossRef](#)]
51. Wang, C.; Sun, D.; Yu, X.; Zhang, X.; Lu, Z.; Wang, X.; Zhao, J.; Li, L.; Yang, X. Cu/Ni nanoparticles supported on TiO₂ (B) nanotubes as hydrogen generation photocatalysts via hydrolysis of ammonia borane. *Inorg. Chem. Front.* **2018**, *5*, 2038–2044. [[CrossRef](#)]
52. Yang, X.; Li, L.; Sang, W.; Zhao, J.; Wang, X.; Yu, C.; Zhang, X.; Tang, C. Boron nitride supported Ni nanoparticles as catalysts for hydrogen generation from hydrolysis of ammonia borane. *J. Alloy. Compd.* **2017**, *693*, 642–649. [[CrossRef](#)]
53. Gao, D.; Zhang, Y.; Zhou, L.; Yang, K. CuNi NPs supported on MIL-101 as highly active catalysts for the hydrolysis of ammonia borane. *Appl. Surf. Sci.* **2018**, *427*, 114–122. [[CrossRef](#)]



© 2019 by the authors. Licensee MDPI, Basel, Switzerland. This article is an open access article distributed under the terms and conditions of the Creative Commons Attribution (CC BY) license (<http://creativecommons.org/licenses/by/4.0/>).